Structural Variants of $Ca_{0.85}CuO_2(Ca_{5+x}Cu_6O_{12})$

O. MILAT*,† G. VAN TENDELOO,* S. AMELINCKX,*
T. G. N. BABU,‡ AND C. GREAVES‡

*University of Antwerp (RUCA), Groenenborgerlaan 171, B2020 Antwerp,
Belgium; †Institute of Physics, University of Zagreb, Bijenicka 46, 41000
Zagreb, Croatia; and ‡School of Chemistry, University of Birmingham,
B152TT Birmingham, United Kingdom*

The structure of $Ca_{0.85}CuO_2$ was reexamined by means of electron diffraction and electron microscopy using the newly developed method of selective imaging in intergrowth structures in which the two substructures are based on different sublattices. The results of previous work are confirmed. Moreover, it is shown that two stacking variants and their twin related structures occur in the calcium "substructure." The copper–oxygen substructure occurs in one variant only; it is often modulated by the various calcium arrangements, leading to "phase" disorder in its modulation pattern. It is shown that the ribbons of CuO_4 clusters are presumably tilted with respect to the (010) plane. © 1992 Academic Press, Inc.

1. Introduction

In a previous paper (*1*) the modulated structure of $Ca_{0.85}CuO_2$ was discussed, and it was shown often to be incommensurate, as could be concluded from the occurrence of orientation and spacing anomalies in the satellite sequences exhibited by the diffraction patterns of a number of specimens. The small and somewhat variable incommensurability was suggested to be related to the nonstoichiometry (*2*), causing mutual modulation of the two "substructures" forming the intergrowth structure, which have different average periods along the b_o direction. It was also suggested that the modulation displacements were small and presumably associated mainly with the calcium substructure, the planes of constant phase being parallel to the $(011)_o$ planes of the basic orthorhombic lattice.

It was also found that two twin-related modulation directions occur and could be attributed to longitudinal shifts of the calcium chains within the "tunnels" in the CuO_2 matrix (*1*). The observation of the latter type of disorder implies that different arrangements of the calcium chains are possible.

In this paper we present evidence that indeed different ordered calcium arrangements within the same CuO_2 matrix are compatible with the observed modulation pattern and actually occur. It was also suggested in (*1*) that the intergrowth structure could be referred to two different separate sublattices: one for CuO_2 and one for Ca. We exploit the spatial separation of the corresponding reciprocal sublattices to image selectively the CuO_2 arrangement on the one hand and the calcium ararngements on the other hand. We hereby use the recently developed method of selective imaging (*3*).
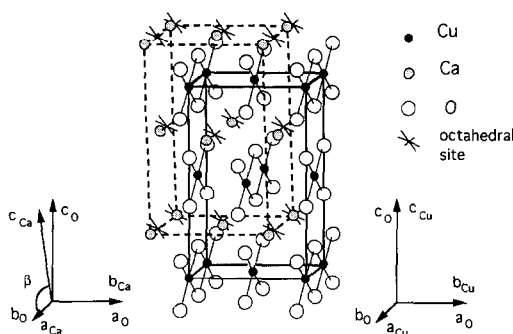
As is shown further below, the different

FIG. 1. Schematic representation of the structure $Ca_{0.85}CuO_2$ with the face-centered orthorhombic unit cell for the CuO_2 sublattice (solid lines) and the "all-face-centered" monoclinic unit cell for the Ca sublattice (dashed lines).

Ca arrangements are based on various monoclinic sublattices, while the Cu arrangement remains orthorhombic. For the sake of self-consistent correlation between these sublattices, we hereafter change the notation for the orthorhombic unit cell parameters (with the label "Cu") from the notation (labeled "o") used previously in (1) and (4), namely:

$$a_{Cu} = b_o = 0.280 \text{ nm};$$
$$b_{Cu} = a_o = 0.632 \text{ nm};$$
$$c_{Cu} = c_o = 1.057 \text{ nm}.$$

This means that we interchange the a and b axes as shown in Fig. 1; this is in agreement with the setting proposed in (5) and (6) and recently used in (7).

The same type of analysis that was applied here, i.e., in terms of two interpenetrating substructures, the copper–oxygen substructure on the one hand, and the cation substructure on the other hand, could be applied also to the series of compounds studied by Davies (7) with nominal compositions $M_{2-x}Ca_{2+x}Cu_5O_{10}$. When the composition of these compounds is written as $(M_{1-x}Ca_x)_{0.80}CuO_2$, it becomes clear that they are more cation deficient than the pure calcium cuprate $Ca_{0.85}CuO_2$ studied here.

It should be noted that the compounds with compositions $(Ca_{0.85}Sr_{0.15})CuO_2$ (8) and $(Sr_{0.85}Nd_{0.15})CuO_2$ (9), in which the ratio (cation/Cu) is unit, have a simple tetragonal structure; as this ratio decreases, the structures become more complicated and are in general incommensurately modulated intergrowth structures (3).

2. Structural Considerations

To make it easier for the reader to follow our considerations, we briefly recall the building principle of the structure, as determined by neutron and X-ray diffraction, in Refs. (4) and (6) and which is shown schematically in Fig. 1.

It can be described as a framework of edge-sharing CuO_4 square planar clusters arranged in ribbons parallel with the a_{Cu} direction and situated in $(010)_{Cu}$ planes, the copper atoms being located on a face-centered orthorhombic lattice. These ribbons form O–Cu–O lamellae parallel with the (001) Cu plane. Within these lamellae the ribbons have a staggered arrangement consistent with the face-centered lattice of the copper atoms. The unit cell contains two such O–Cu–O lamellae related by a displacement vector $\frac{1}{2}$ $[a_{Cu} + c_{Cu}]$, due to face centering of the copper arrangement. Within this CuO_2 framework the oxygen atoms limiting two successive O–Cu–O lamellae form rows of edge-sharing, slightly deformed octahedral interstices, which can be occupied by calcium atoms. As suggested in (4) and shown by means of high-resolution electron microscopy in (1), roughly only 5 of 12 potential positions are occupied in such a way that five Ca–Ca separations along the chain direction correspond with six Cu–Cu separations in the ribbons. The position of the Ca chain configuration as a whole, with respect to the CuO_2 framework, can easily be changed along the a_{Cu} direction, by small longitudinal displacements of the individual calcium atoms. A small displacement of the

Ca chain with respect to the CuO_2 framework results in a much larger shift of the phase of the combined configuration of the Ca and CuO_2 substructures.

In Ref. (1) we have shown that a long period modulated structure results in a modulation vector very close to $\frac{1}{12}$ $[202]^*_{Cu}$; in fact, it is often incommensurate. The planes of constant phase of the modulation pattern are thus in $(10\bar{1})_{Cu}$ or $(101)_{Cu}$ planes, leading two twin related modulation variants.

In Ref. (1) the structure was described with respect to an approximate monoclinic superlattice unit cell with the a_m lattice parameter equal to the smallest common multiple of the Ca–Ca and Cu–Cu separations, i.e., $\mathbf{a}_m = 6\mathbf{a}_{Cu}$ $(=5\mathbf{a}_{Ca})$; $\mathbf{b}_m = \mathbf{b}_{Cu}$; $\mathbf{c}_m = \mathbf{a}_{Cu} + \mathbf{c}_{Cu}$. However, we also pointed out that, alternatively, the two substructures could be described with respect to two separate, but closely related sublattices. The copper–oxygen lattice is face centered orthorhombic with the cell parameters (4,6): $a_{Cu} = 0.280$ nm; $b_{Cu} = 0.632$ nm; $c_{Cu} = 1.057$ nm. The average Ca arrangement in $Ca_{0.85}CuO_2$ can be related to a monoclinic sublattice with the cell parameters $a_{Ca} = (1/0.85)$ $a_{Cu} = 0.330$ nm; $b_{Ca} = 0.632$ nm; $c_{Ca} = 1.058$ nm; $\beta_{Ca} = 87°$ (Fig. 1).

The latter nonprimitive (all-face-centered) unit cell is the one which is most closely related to that of the copper sublattice; it is slightly monoclinic, the c axis enclosing an angle of 3° with the corresponding axis of the copper arrangement. A smaller unit cell, based on a Bravais lattice, can be defined as discussed under structural Models.

All strong "superlattice" reflections appearing in X-ray powder diffraction patterns represented in Fig. 2. in Ref. (4) could be indexed on the basis of the nonprimitive, all-face-centered monoclinic cell (Fig. 1) of the cation sublattice, explicitly: 111_{Ca}, $11\bar{1}_{Ca}$, 113_{Ca}, $11\bar{3}_{Ca}$, . . . (1). Such a simple interpretation is not given to the lines in Fig. 2

and Table I in Ref. (7) for the analogous reflections of $Ca_{2+x}Y_{2-x}Cu_5O_{12}$, although this is possible, when referring to the cation sublattice cell, as in our analysis.

According to the apparent similarities between the diffraction patterns of $Cu_{0.85}CaO_2$ and $M_{2+x}Ca_{2-x}Cu_5O_{10}$ $(M = Y, Nd, Gd)$, a similar description has to hold for the latter compounds, although the cations are now distributed over 4 of 10 potential octahedral positions instead of over 5 of 12. Four cation separations would thus correspond with 5 copper separations along the chain direction.

However, the average cation sublattice in the rare-earth cuprates (7), $(RE_xCa_{1-x})_{0.80}CuO_2$, has a different lattice parameter, a_{ct}, which is close to but not exactly what one would expect on simple grounds, $a_{ct} = (1/0.8)$ $a_{Cu} = 0.355$ nm, and moreover varies with x (7). (The label "ct" is used to refer to the cation sublattice in "mixed" cuprates.)

3. Experimental

$Ca_{0.85}CuO_2$ material was synthesized from high-purity $CaCO_3$ and CuO using conventional solid state techniques. Intimate mixtures were heated for two periods of 16 hr in flowing oxygen at 800°C with an intermediate regrind (4). The detailed procedure was given in (4). It should be emphasized that the preparation was aimed at achieving as closely as possible the stoichiometric composition $CaCuO_2$. It turns out that the ratio Ca/Cu = 0.85 is the largest ratio that could be realized.

Electron microscopy samples were prepared by further crushing and dispersing the powder on a copper grid dipped in a liquid glue.

4. Reciprocal Space

4.1. Observations

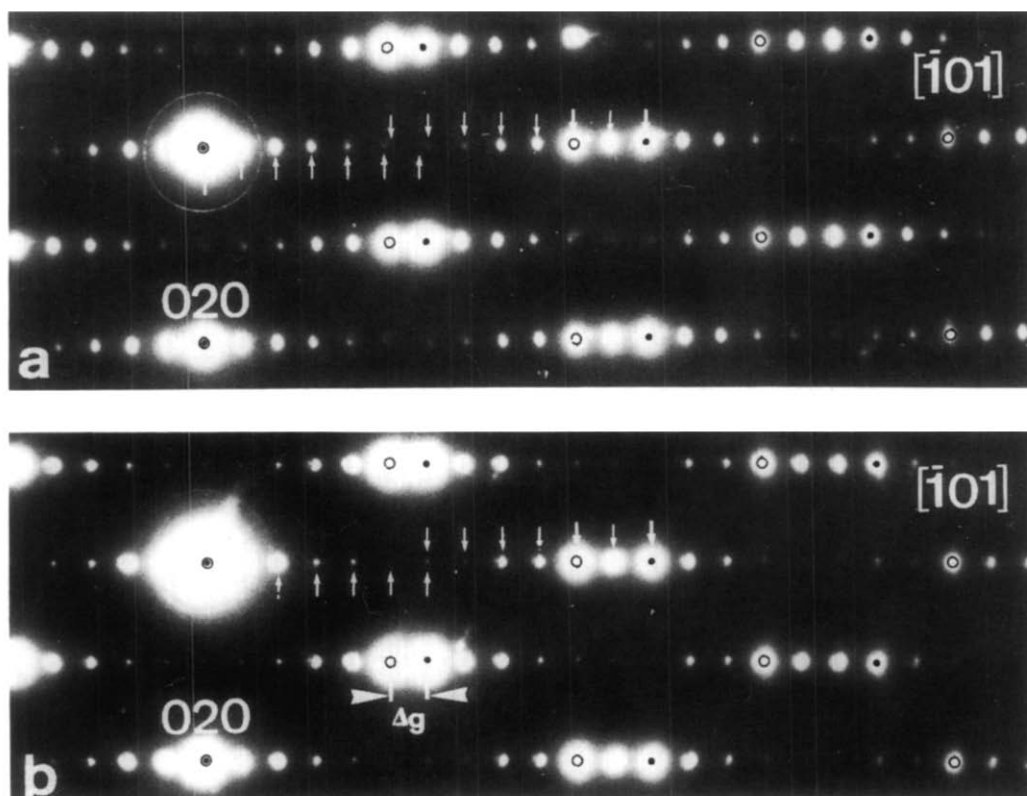Detailed exploration of reciprocal space by tilting the specimen confirmed the possi-

FIG. 2. Comparison between the diffraction patterns along the [101] zone of $Ca_{0.85}CuO_2$ of the incommensurate form (a) and the commensurate form (b). The sequences of satellite spots, indicated by arrows, exhibit a spacing anomaly in a, while they do not in b. Note the two meshes defined by the positions of the most intensive spots belonging to the two sublattices; the open dots indicate spots due to the calcium sublattice, whereas the closed dots refer to the copper–oxygen sublattice. The vector Δg which generates the satellites is indicated.

bility of describing the complete reciprocal lattice as the superposition of two distinct reciprocal lattices which are generally incommensurate, one describing the translation symmetry of the copper–oxygen framework and the other one that of the average calcium arrangement, as shown in Fig. 1. However, it was found that in well-ordered specimens the structure is sometimes commensurate over appreciable areas. We therefore consider in particular this commensurate structure, the diffraction pattern along the $[\bar{1}01]_{Cu}$ zone of which is illustrated in Fig. 2b and compared with an incommensurate diffraction pattern along the same

zone and of the same type as that considered previously (1) (Fig. 2a). The ideal stoichiometric composition in the commensurate case, according to Fig. 2b, would be Ca_5 Cu_6O_{12}, i.e., $Ca_{0.833}CuO_2$. We also sometimes observed diffuses "relplanes" perpendicular to the Ca chain direction and passing through the nodes of the copper–oxygen reciprocal lattice, for instance, as shown in Fig. 3.

4.2. Interpretation

We now discuss these observations in more detail. In Fig. 4 we have reproduced the $[010]_{Cu} = [010]_{Ca}$ zone diffraction pat-
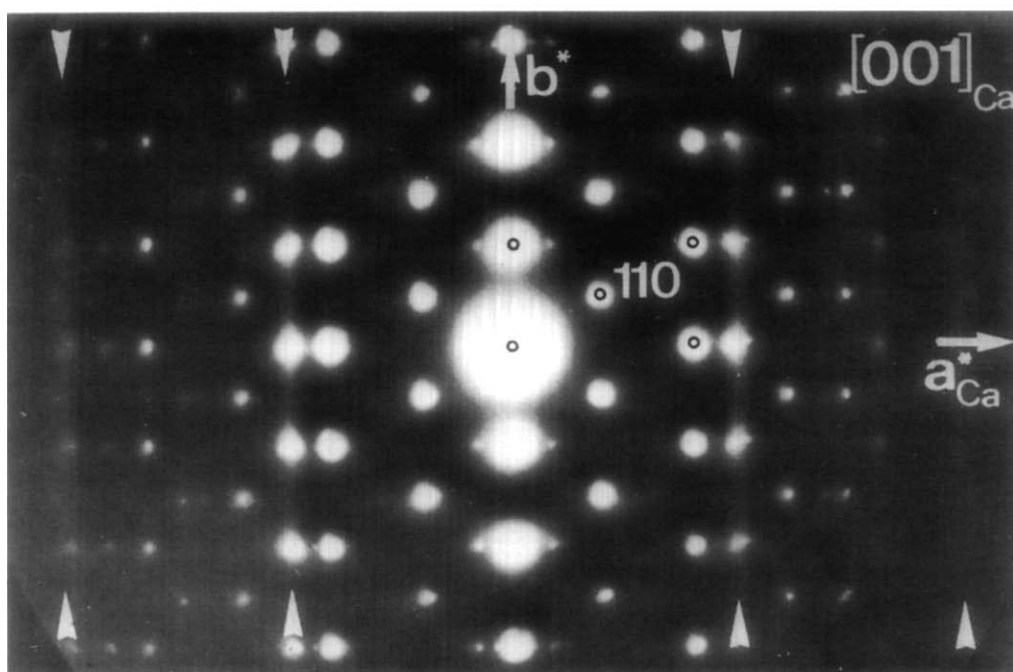
FIG. 3. Diffraction pattern of $Ca_{0.85}CuO_2$ along the $[001]_{Ca}$ zone. Note the presence of diffuse lines through the rows of copper spots, indicated by arrows; these lines are traces of "relplanes" perpendicular to $[100]_{Cu}$.

tern and we have indicated by labels "a" to "d" the most characteristic sections along which diffraction patterns were obtained by tilting around the [010] zone axis; these patterns are reproduced in Figs. 5a–5d correspondingly.

From a number of such patterns taken at very small angular intervals as viewed along the [010] zone axis, we have constructed the reciprocal space represented in Fig. 6a, for the simplest situation. Usually twinning of the type already described in Ref. (1) complicates the patterns (Fig. 6c), as we shall see further below.

The electron diffraction patterns (Figs. 5a–5d) are not entirely consistent with the reciprocal space sections to be expected on the basis of the structure proposed in Ref. (1) and represented by the reciprocal lattice projection in Fig. 6a. For this structure model the copper–oxygen, as well as the

calcium, sublattices are both face centered in direct space (Fig. 7a), and, hence, the reciprocal lattice would be body centered for both substructures (Fig. 6a). From the diffraction patterns in Fig. 5, one can see that this is indeed still the case for the copper sublattice, for which only spots with unmixed indices appear as strong spots and, thus, it remains face centered orthorhombic (at least to a good approximation, as we shall see below). However, the reciprocal calcium sublattice exhibits sometimes relatively intense spots which would be forbidden for a face-centered lattice, thus suggesting that the Ca sublattice is C face centered (Fig. 6b). This can, for instance, be concluded from Fig. 3 and Fig. 5b both of which represent the $[001]_{Ca}$ section designated "b" in Fig. 4. The intensity of the 110_{Ca} spot indicated in the center of the rectangular mesh in Fig. 3 and Fig. 5b differs
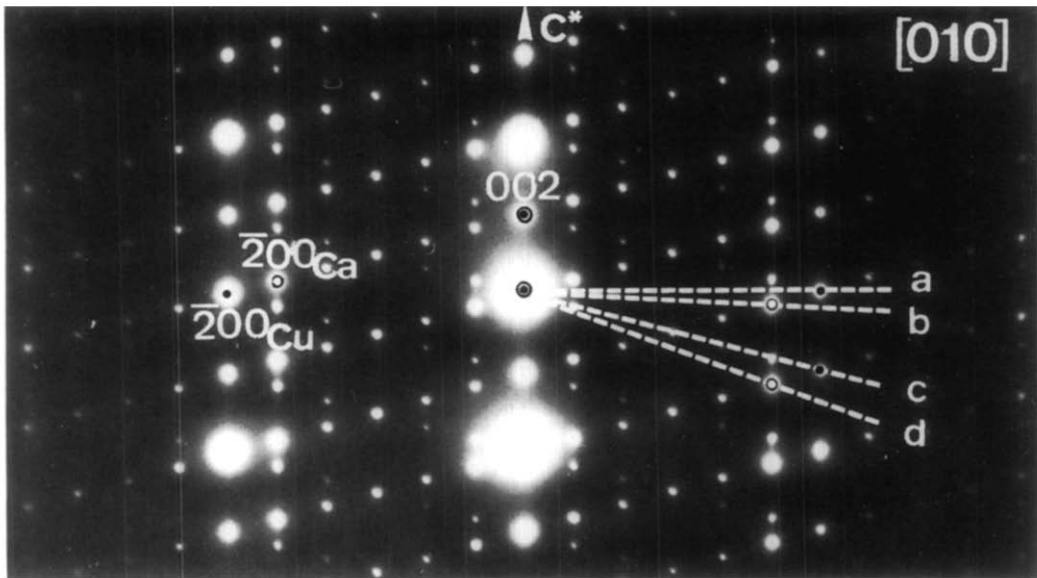
FIG. 4. Diffraction patterns along the $[010]_{Cu}$ zone of $Ca_{0.85}CuO_2$. This section contains twin-related sequences of "satellites;" the odd order satellites are extinct. Note that every third row parallel to c^* consists of unsplit spots. The dashed lines a, b, c, d indicate the traces of the sections in Fig. 5.

for diffraction patterns taken in different areas of the specimen. This clearly means that, in some areas, a variant structure exists in which the Ca substructure is built on a monoclinic C-face-centered Bravais lattice with $\beta = 87°$ (Fig. 7b), rather than on a face-centered, redundant one corresponding with a C-face-centered Bravais monoclinic lattice with $\beta = 105°$ (Fig. 7a). Moreover, a number of weak as well as a few strong spots in electron diffraction patterns remain unaccounted for. It was therefore necessary to take into account twinning of both types of calcium sublattices as demonstrated in Figs. 6c and 6d. This leads to the reciprocal space schematically represented in Fig. 6e, which now accounts for all observed spots.

The satellite sequences along the $[101]^*_{Cu}$ direction (Fig. 4 and Fig. 5c), and also along the twin-related $[10\bar{1}]^*_{Cu}$ direction, can be attributed either to double diffraction or to mutual modulation of the two substructures

in the way described in (10). It is not obvious how the two effects could be distinguished since the geometry of the resulting diffraction patterns is the same for both cases. The sequences of satellite spots can formally be generated by repeatedly applying the difference diffraction vector $\Delta g = \frac{1}{6}[101]_{Cu}$ (indicated in Fig. 2 and in Fig. 6a) to all basic spots; Δg is the vector connecting the 111_{Cu} node with the 111_{Ca} (or $11\bar{1}^{(T)}Ca$) node. The interpretation in terms of two sublattices, rather than as a simple modulation of one of the two sublattices, for instance, the copper–oxygen one, is supported by the observation that the decrease in intensity of the satellites with increasing distance from their "center of gravity" is *not* monotonous. The relative intensities of the satellites are most clearly visible in Fig. 2 (and also in Fig. 5c). The most intense spots coincide with node points of the sublattices; the weaker spots can be attributed to double diffraction or mutual modulation.
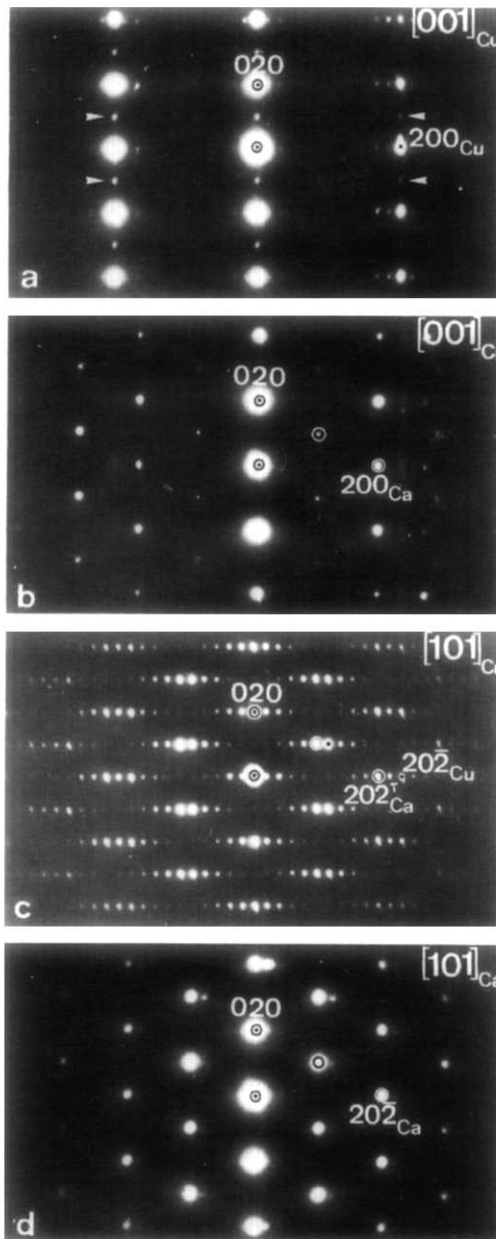
FIG. 5. Diffraction patterns along different sections of reciprocal space of $Ca_{0.85}CuO_2$ obtained by tilting around [010]: (a) $[001]_{Cu}$ zone revealing the reciprocal section containing only the copper–oxygen spots (besides common spots along the b^* axis). Note the presence of spots of the type: $hk0$ with h = even, k = odd (indicated by arrowheads); (b) $[001]_{Ca}$ zone revealing the section which contains only the calcium sublattice spots (besides b^* axis). Note the absence of spots of the type mentioned in (a); (c) $[101]_{Cu}$ zone revealing the section which contains the spots of both sublattices (Cu plus either one of the two twin variants of the Ca sublattice) and the sequences of satellite spots. Closed and open dots indicate the basic spots of the CuO_2 and the Ca sublattices, respectively; (d) $[101]_{Ca}$ zone. Section with only Ca sublattice spots.
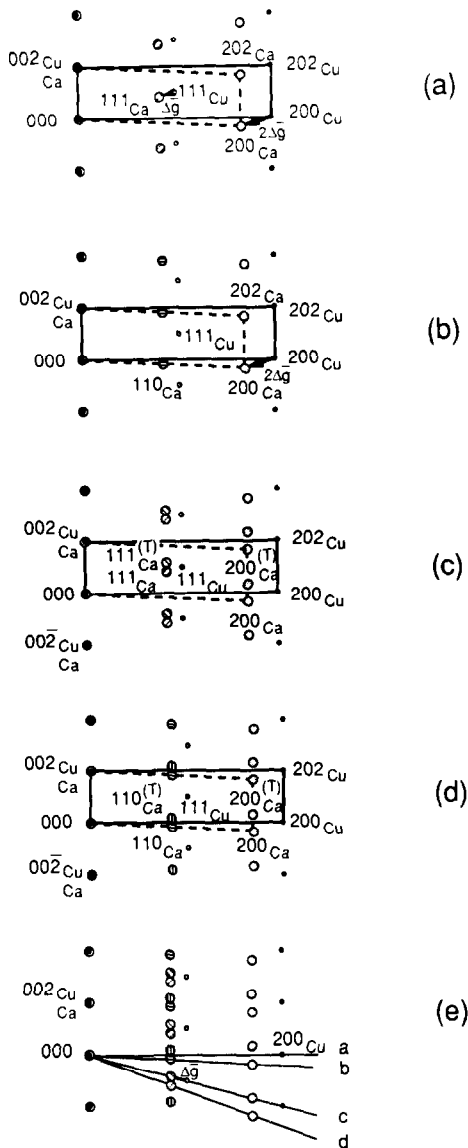
FIG. 6. Schematic representation of the reciprocal space projection along [010]* for the two types of structures of $Ca_{0.85}CuO_2$ which correspond to the two stacking modes of calcium arrangement. (a) Type I stacking mode; (b) type II stacking mode; (c) two twin-related variants of the type I stacking mode; (d) two twin-related variants of the type II stacking mode; (e) the four structural variants are superimposed to represent the complexity of the reciprocal space as usually observed. Lines a, b, c, d indicate the traces of sections in Fig. 5 corresponding to those in Fig. 4. Smaller and larger dots represent spots belonging to the CuO_2 and the Ca sublattices, respectively.
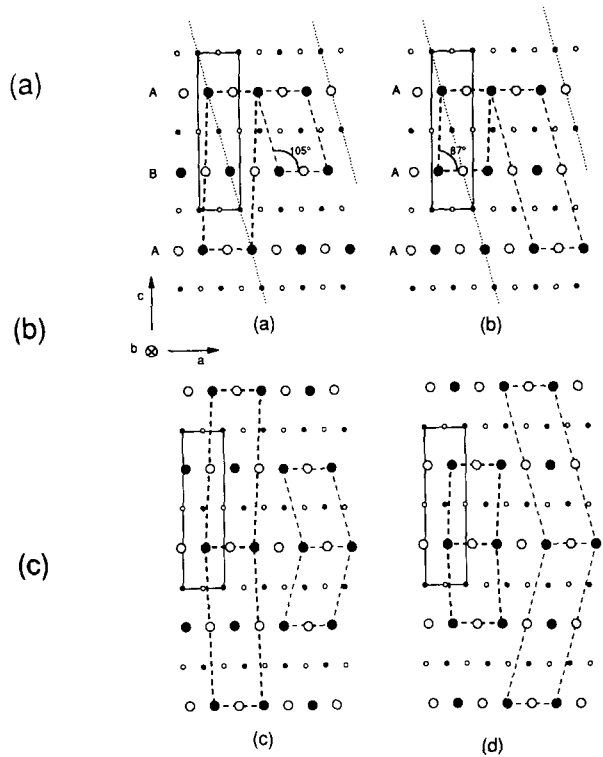

FIG. 7. Structure models for $Ca_5Cu_6O_{12}$, assuming different stacking modes for the calcium chains. Small and large dots represent Cu and Ca atoms; closed dots, in the plane; open dots, above or below the plane. (a) Type I stacking of the calcium chains; (b) type II stacking of the calcium chains; (c) reflection twin on (001) for type I Ca stacking within the untwinned CuO_2 framework; (d) reflection twin on (001) for type II Ca stacking within the untwinned CuO_2 framework. The dotted lines in (a) and (b) indicate the planes of equal constant phase for the Ca and CuO_2 sublattices. The unit cells are outlined by solid and dashed lines for the copper–oxygen and the calcium sublattices, respectively; cells indicated by heavy dashed lines are referred to in the text as unit cells; Ca cells indicated by lightly dashed lines have their (100) faces parallel with the planes of constant phase.

From Fig. 2, it is obvious that the separation of the two most intense spots (indicated by closed and open dots) in each of the satellite sequences increases stepwise by Δg with increasing distance of the satellite sequence from the $0k0$ row of spots. This is also visible in the (010)* section of Fig. 4, where the two

most intense spots are separated by $2\Delta\mathbf{g}$, as indicated in Figs. 6a and 6b; note that the odd order reflections are extinct along this zone (Fig. 4). This geometry of the intense spots is exactly what one expects if the reciprocal space consists of the superposition of two reciprocal lattices with a different lattice parameter along the horizontal direction in Fig. 2. The weaker spots are then due to double diffraction and (or) mutual modulation of the substructures (10).

Summarizing this discussion, we can state that the reciprocal lattice shows that the copper sublattice is in all specimens the same, face centered orthorhombic, as described in Ref. (1) and (4). However, the calcium sublattice is complicated by the occurrence of two different calcium arrangements, both based on a monoclinic lattice and both arrangements exhibiting twinning: one of the arrangements (type I) is based on a nonprimitive all-face-centered monoclinic unit cell described with reference to the orthorhombic sublattice by the base vectors

$$\mathbf{a}_{Ca} = 6/5\mathbf{a}_{Cu}; \quad \mathbf{b}_{Ca} = \mathbf{b}_{Cu};$$
$$\mathbf{c}_{Ca} = 1/5\mathbf{a}_{Cu} + \mathbf{c}_{Cu}.$$

This structure is schematically shown in projection along the **b** axis in Fig. 7a; this sublattice was discussed in Ref. (1).

The other one (type II) is based on a smaller C-face-centered monoclinic lattice the base vectors of which are given with respect to the same copper sublattice by the relations

$$\mathbf{a}_{Ca} = 6/5\mathbf{a}_{Cu};$$
$$\mathbf{b}_{Ca} = \mathbf{b}_{Cu}; \quad \mathbf{c}_{Ca} = 1/2(1/5\mathbf{a}_{Cu} + \mathbf{c}_{Cu}).$$

This structure is schematically shown in projection along the **b** axis in Fig. 7b.

5. Structural Models

5.1. Calcium Arrangements

There is apparently no reason to question the overall structure of the copper–oxygen

framework as represented in Fig. 1. The discussion can therefore be restricted to the different possible stacking modes of the calcium chains within this framework. It was pointed out previously (1) that different stacking modes are possible, leading, for instance, to twinning of the calcium sublattice. (It is worth noting that the observation of well-defined calcium columns in Fig. 8 of Ref. (1) is consistent with a longitudinal displacement of certain Ca chains, provided that the displacement is half of the Ca–Ca separation in a chain. Such displacements would not affect the straightness of the Ca columns.)

The structure, as reported in (1), is clearly the one which gives rise to the type I reciprocal lattice schematically shown in Fig. 6a); in direct space, it can be represented schematically as in Fig. 7a, as viewed along the [010] direction (for simplicity the oxygen atoms are not shown in Fig. 7). The "planes of constant phase" for the complete structure, which determine the direction and spacing of the "satellite" sequences, are parallel to the $(101)_{Cu}$ planes of the copper sublattice, as indicated by the trace marked in Fig. 7a. Their projected spacing along this zone is clearly half their actual spacing, which explains the systematic extinctions of the odd order satellites in the diffraction pattern made along this zone (Fig. 4). An alternative manner of explaining the same feature is to say that the commensurate composite structure has a glide mirror plane parallel to the (010) plane, when described with respect to the $Ca_5Cu_6O_{12}$ superlattice unit cell, as was done in Ref. (1). The geometry of the satellite sequences, i.e., their orientation and spacing, is thus consistent with the structure of type I.

The alternative structure, which leads to the type II reciprocal lattice (Fig. 6b), is obtained from the type I structure by shifting every other (001) calcium layer over one-half of the Ca–Ca separation distance along the chain direction (Fig. 7b). This results in

halving the c parameter and the structure is now based on a smaller C-centered monoclinic unit cell. In projection along the [010] zone the structure looks the same as that of type I. It is therefore again consistent with the extinction of the odd order satellites when viewed along this zone. As a nonprimitive unit cell of the calcium sublattice, one can choose either a redundant all-face-centered monoclinic cell outlined in Fig. 7b or a twofold C-face-centered monoclinic one. The latter cell is closely related to the Cu orthorhombic unit cell, whereas the former one has faces which are parallel to the planes of equal phase. Both redundant cells contain two C-centered unit cells of a Bravais lattice.

We can designate the two positions of the calcium layers within the same CuO_2 matrix as A and B; they differ by a displacement vector $\mathbf{R} = \frac{1}{2}[100]_{Ca}$. The type I structure can then be represented by the notation . . .ABAB. . . , whereas the type II structure would be designated . . .AAA. . . or . . .BBB. . . . It is to be expected that more complicated sequences, such as . . .AABAAB. . . , may occur. Faulty sequences would give rise to streaks along the $\mathbf{c}^*_{Ca}$ direction associated with the reflections $\mathbf{g}$ (referring to the calcium reciprocal lattice) for which $\mathbf{g} \cdot \mathbf{R} = \frac{1}{2}(\text{mod } 1)$, i.e., for h odd. These are the reflections in the center of the rectangle of intense spots in Fig. 5b; these reflections are indeed streaked, as has been found by means of tilting experiments.

It is clear that both structures can be formed within the same copper–oxygen matrix in two versions, the two variants being related by a mirror operation with respect to the (001) plane, which is a mirror plane for the copper sublattice but not for the calcium sublattice. In both cases the planes of the constant phase also adopt orientations related by a mirror operation with respect to the (001) plane, as represented in Figs. 7c and 7d and in reciprocal space in Figs. 6c and 6d. Low-resolution lattice fringes exhib-

iting the modulation wave fronts were reproduced in Fig. 8b of Ref. (1). Since these images exhibit the same geometrical features for the twins of both types of structures, they give no indication of the stacking mode of the calcium chains. We demonstrate that high-resolution selective imaging (3) of the calcium substructure allows us to confirm the occurrence of the two stacking modes.

5.2. Geometrical Considerations

The presence of the sequences of sharp satellite reflections proves that the planes of constant phase (PCP) are well determined and are defined primarily by the orthorhombic copper–oxygen sublattice since they are parallel to planes of this sublattice with very simple indices: $(101)_{Cu}$ and $(\bar{1}01)_{Cu}$ planes. The observations further require that the calcium lattice be compatible with these planes of constant phase (either $10\bar{1})_{Cu}$ or $(101)_{Cu}$, corresponding with the observed twins). However, the intrachain spacing a_{Ca} is different from a_{Cu}, whereas b_{Ca} and b_{Cu} are identical, and c_{Ca} and c_{Cu} are nearly equal.

The various requirements can be reconciled only by assuming a monoclinic arrangement of the calcium ions; the monoclinic angle of the sublattice is given by the relation $\tan \beta = c_{Cu}/(a_{Ca} - a_{Cu})$, as can be deduced from Fig. 8a. In the specific case of $Ca_5Cu_7O_{12}$, $6a_{Cu} = 5a_{Ca}$ and we have $\tan \beta = 5c_{Cu}/a_{Cu}$. This is indeed the observed monoclinic angle of the calcium sublattice. These geometrical relations suggest that the phase of the Ca chains must be rather strongly and rationally correlated with the orthorhombic copper–oxygen sublattice. The positions occupied by the calcium atoms within the octahedral interstices situated along a given $(101)_{Cu}$ (or $(10\bar{1})_{Cu}$) plane (Fig. 8b) must be the same for all chains in a given variant, possibly modulus $\frac{1}{2}a_{Ca}$, however. It should be noted that the planes of constant phase, as viewed along the [010] direction, remain invariant if the Ca chains
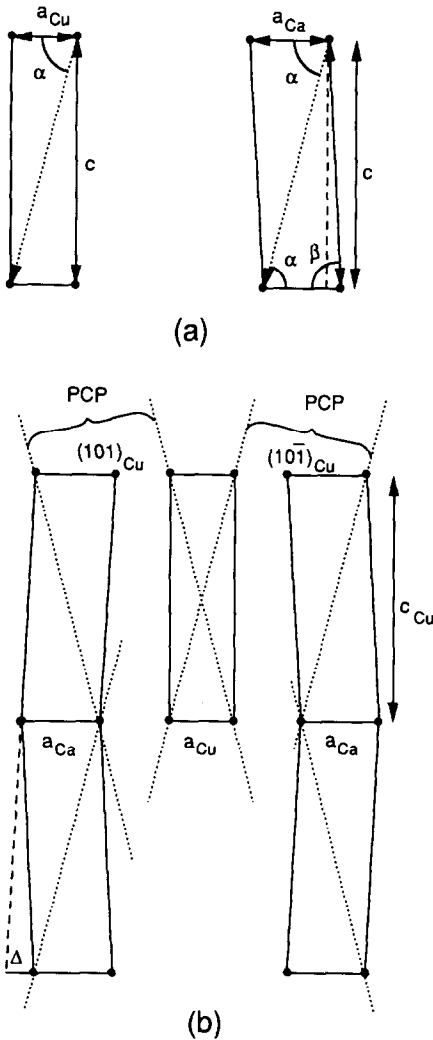
(a)

(b)

FIG. 8. Derivation of the geometrical relations between the copper–oxygen and the calcium sublattices in $Ca_5Cu_6O_{12}$. The orientations of the planes of constant phase (PCP) are indicated in the two sublattices as well as their twins.

are shifted longitudinally over $\frac{1}{2}a_{Ca}$, since this is the projected repeat distance along the chains.

These rational relationships are also apparent from the twin diffraction pattern along the [010] zone (Fig. 4), in which every third spot row, parallel with the [00l]* un-split central row, is found to be unsplit as well. This is directly related to the fact that the twinning vector Δ(Fig. 8b) is a simple rational fraction of Δ:$a_{Ca} = \frac{1}{3}$. This suggests that twinning can be brought about by shifting calcium chains in successive (001) planes over Δ, 2Δ (= $-\Delta$), 3Δ (= 0), . . . along the a_{Cu} direction; i.e., small displacements over Δ of the chains can bring about twinning.

5.3. Oxygen Arrangement

It is interesting to note that in the diffraction pattern along the $(001)^*_{Cu}$ section in Fig. 5a, the reflections $hk0$ with h = even and k = odd are relatively weak, but present (indicated by arrows), violating the extinction criteria for an all-face-centered orthorhombic lattice. However, the $0k0$ reflections with k = odd are not present in sections of the calcium sublattice (Fig. 5b) obtained from the same area by tilting about the [010] zone axis (from "a" to "b" in Fig. 4). This suggests that the copper–oxygen sublattice is not strictly face centered orthorhombic, the deviation being such that these forbidden spots are weakly present. This could, for instance, be due to a small tilt of the planar CuO_4 ribbons about their length axis. A possible scheme is represented in an exaggerated manner in Fig. 9, as viewed along c_{Cu} and a_{Cu} axes. Such tilts would not directly affect the $h00$, $0k0$, and $00l$ rows of spots, but they would affect the noncentral rows such as $2k0$ and $\bar{2}k0$, present along the diffraction zone in Fig. 5a. The additional spots with k = odd along the $0k0$ row would then result from double diffraction out of the $2k0$ row.

The postulated displacements of the oxygen atoms are in agreement with the neutron diffraction results in (4), which showed that the thermal agitation ellipsoid associated with the oxygen atoms is highly anisotropic with its largest axis parallel to the [0k0] direction. We assume that the lattice of the copper atoms remains orthorhombic face
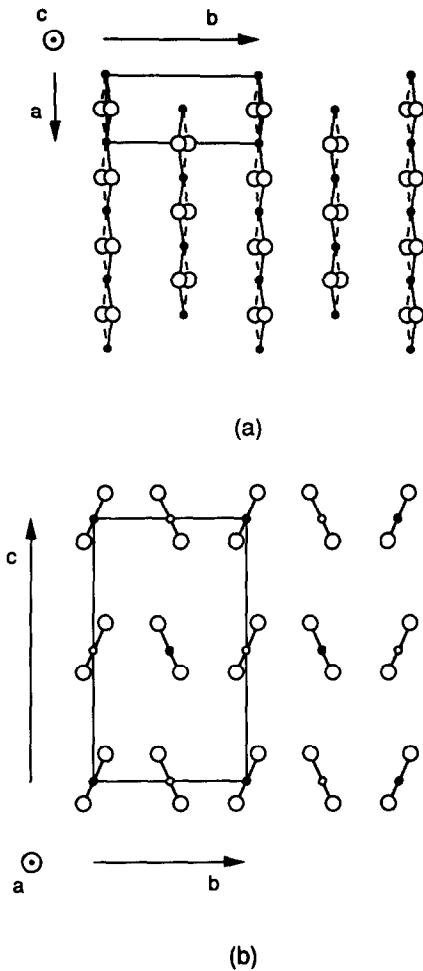
(a)

(b)

FIG. 9. Illustration of the proposed tilt pattern of the CuO_4 squares in the CuO_2 ribbons: (a) as viewed along [001]; (b) as viewed along the length axis of the ribbons: [100]. Small dots represent copper, large dots represent oxygen.

centered and the tilts of the oxygen squares are all in the same sense along a given (010) layer. The body-centered reciprocal lattice of the copper arrangement must then be complemented by the contribution of the oxygen arrangement. The oxygen arrangement is based in direct space on a B-face-centered orthorhombic lattice of the copper and oxygen arrangements is then as observed in Fig. 5a; the most intense spots

originate from the copper arrangement; the weak spots are due to the tilted oxygen arrangement; the spots $0k0$ with $k = $ odd are kinematically extinct but produced by double diffraction out of the $2k0$ row. This is consistent with their absence in the central row in the Ca sections (Figs. 5b and 5d).

6. High-Resolution Imaging

In Ref. (3) it was shown that by a proper choice of the reciprocal lattice sections one can separately image the two substructures of a composite intergrowth structure. In the present case, we are interested mainly in the geometry of one of the sublattices, i.e., the calcium sublattice, and it is therefore of interest to image this substructure selectively for each of the two types of structures as characterized by their reciprocal lattices.

From Fig. 4 we can deduce that the $(001)^*_{Ca}$ section indicated by label "b" and the $(101)^*_{Ca}$ section indicated by label "d" are suitable for revealing the calcium arrangement selectively (3), since the electron diffraction patterns along these sections (shown in Figs. 5b and 5d, respectively) contain only spots of the Ca sublattices. These sections are composed of the diffraction patterns with different unit meshes for the two structural variants. This can be concluded by comparing the intensity of the spot in the center of the rectangular mesh, indicated as 110_{Ca} in Fig. 3, with the corresponding spot in Fig. 5b, as both diffraction patterns are taken along the same $[001]_{Ca}$ zone. In the diffraction pattern along the $[001]_{Ca}$ zone for the type I structure the unit mesh is a primitive rectangle with no 110_{Ca} spot, as can be deduced from Fig. 6a, whereas for the type II structure, the unit mesh is a centered rectangle, indicated by the 110_{Ca} spot on the dashed line connecting 000 and 200_{Ca} in the [010] projection (Fig. 6b).

A high-resolution image along $[001]_{Ca}$ which selectively reveals the Ca arrangement in the $Ca_{5+x}Cu_6O_{12}$ structure is shown
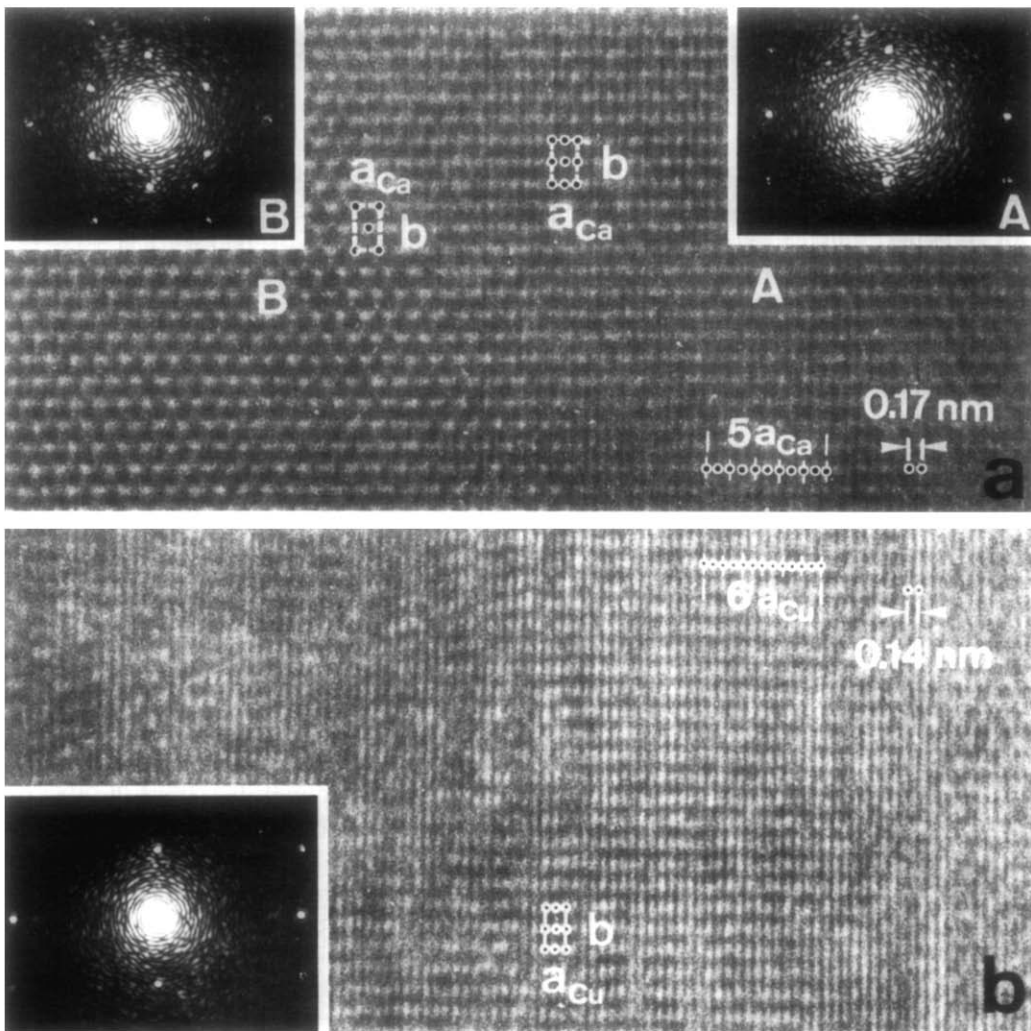
FIG. 10. High-resolution selective images of substructures in $Ca_5Cu_6O_{12}$. (a) Along the $[001]_{Ca}$ zone of an area containing the two stacking modes of the calcium sublattice. In A, stacking mode—type I—two dots per a_{Ca} reveal staggering of the Ca chains; in B, stacking mode—type II—a single dot per a_{Ca} reveals the alignment of Ca chains. (b) Along the $[001]_{Cu}$ zone of the same area as that in a. The bright dot pattern reveals the positions of Cu atoms in the projected structure of the face-centered orthorhombic CuO_2 sublattice. The optical diffraction patterns in the insets can be compared with the corresponding electron diffraction pattern in Fig. 3 and Figs. 5a and 5b, and with the computed patterns in Figs. 11c and 11d.

in Fig. 10a (as imaging along the $[001]_{Ca}$ direction). The corresponding diffraction pattern is Fig. 3; it contains the type II arrangement of spots.

Two different patterns of bright dots can

clearly be recognized in Fig. 10a: the rectangular one in the region labeled "A" and the "hexagonal" one in the region labeled "B". There is a relatively sharp boundary between these regions; the type B pattern cov-

ers only a small fraction of the total area in which type A prevails. Optical diffraction patterns from the corresponding areas of the high-resolution negative are given as insets A and B, respectively. The diffractogram in B has an additional spot in the center of the rectangular mesh of spots, which has the same shape and size as the unit mesh in A. In the image, the vertical spacing (along the [010] direction) is the same in A and B (0.316 nm = $b/2$); the horizontal separation of bright dots (along the $[100]_{Ca}$ direction) in B is equal to $a_{Ca} = 0.33$ nm and twice as large as the corresponding separation in A. In B the dots form a centered rectangle, whereas in A the same rectangle has dots also in the centers of the edges due to the all-face-centered lattice. Therefore the dot separation of 0.17 nm corresponds with half the Ca–Ca spacing along the a_{Ca}.

By selective imaging along the $(001)^*_{Cu}$ section of the same area, the projected structure of the face-centered octahedral CuO_2 sublattice is clearly discernible in Fig. 10b. The spacing between the horizontal rows of bright dots is 0.316 nm, i.e., the same as that for the Ca sublattice, but the spacing between the dots within these rows corresponds with half the Cu–Cu separation along a_{Cu}: 0.14 nm = $\frac{1}{2} a_{Cu}$.

As we show in the paragraph on computer simulation, these two types of bright dot patterns in Fig. 10a reveal the two types of Ca arrangements in the projected structure of the $Ca_5Cu_6O_{12}$, as can be seen in Fig. 11. It is clear that in the type I structure a rectangular arrangement of dots (Fig. 11a) represents the geometry of the columns of calcium atoms as viewed along the $[001]_{Ca}$ direction. This projection is consistent with the face-centered monoclinic arrangement of the calcium atoms.

The projection of the type II structure (Fig. 11b), as viewed along the same direction, consists of a quasi-hexagonal (centered rectangular) pattern. This projection is consistent with the C-face-centered monoclinic

arrangement of the calcium atoms in the type II structure. Cu and O atoms are projected onto the nearly continuous horizontal strings of points for both stacking variants of Ca atoms in Fig. 11. The computed dynamical diffraction patterns and the corresponding simulated images for the two types of Ca arrangements in $Ca_5Cu_6O_{12}$ are also presented in Fig. 11.

Regarding the observed high-resolution image in Fig. 10a, we can conclude that two different Ca arrangements occur since viewing the structure along the same direction leads to different dot configurations in adjacent areas. It should be noted that we convinced ourselves that this observation was not due to local differences in the diffraction conditions, leading to the excitation of spots belonging to a higher Laue zone in certain areas. This conclusion is thus quite independent of any theoretical interpretation. That the difference is due to the calcium arrangements can be deduced from the particular choice of the reciprocal lattice section used for imaging and also from the fact that when using the "homologous" section— $(001)^*_{Cu}$—selectively revealing the copper arrangement (3), one finds the same configuration of dots all over the area (Fig. 10b).

It is found that in most specimens the two types of structure occur simultaneously: type I dominantly and type II in (adjacent) small domains (as B in Fig. 10a). This is reflected in the diffraction pattern by a variable intensity of the 110_{Ca} spot (compare Fig. 3 with Fig. 5b), when selecting different specimen areas. This makes a clear choice of the section to be used for imaging the difference difficult, since it is not sharply defined by the absence or presence of the central spot. Moreover, the diffraction patterns and hence also the images are complicated by the almost inevitable presence of twins. The image in Fig. 10a nevertheless unambiguously demonstrates the existence of the two stacking variants, both of which are compatible with a long period modulated
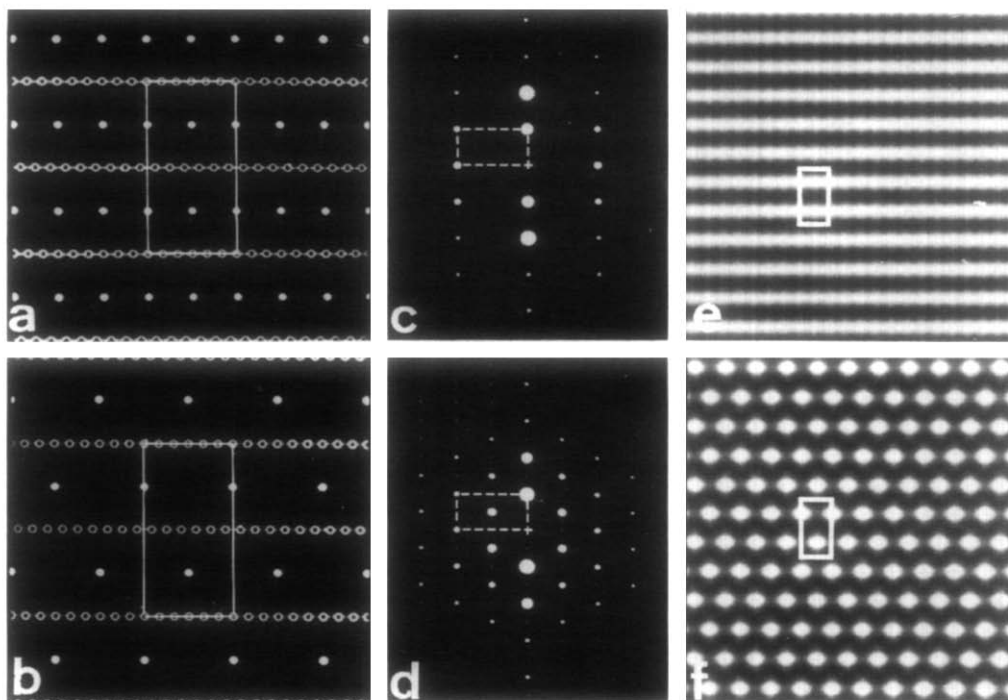
FIG. 11. Computer-generated projected atom positions along the $[105]_m$ of the commensurate monoclinic superlattice of $Ca_5Cu_6O_{12}$ for (a) type I stacking and (b) type II stacking of the calcium atoms. Computed dynamical diffraction patterns of the structures represented in (a) and (b) along the same zone: (c) type I stacking and (d) type II stacking of the calcium atoms. Computer-simulated images along the same zone as the diffraction pattern in (c) and (d) and the projected structure in (a) and (b), respectively. (e) type I stacking and (f) type II stacking of the calcium atoms.

structure having the same set of planes of equal phase.

The selective imaging of one of the substructures (3) is illustrated also in Fig. 12, where a homologous pair of images was taken along the $(101)^*_{Cu+Ca^T}$ section (diffraction pattern, Fig. 5c) and along the $(101)^*_{Ca}$ section (diffraction pattern, Fig. 5d).

By imaging along the common section $(101)^*_{Cu+Ca^T}$ (Fig. 12a), both sublattices are displayed; the brightness modulation fringes along [010] reveal the mutual modulation of the two sublattices perpendicular to [010]. It was shown (1) that the bright dots in the thin region of the wedge-shaped specimen area represent the Cu columns; in the thicker region the Ca columns are repre-

sented by bright dots while the less bright dots reveal the positions of the Cu columns. In Fig. 10a, both types of atoms are clearly discernible in the region of intermediate thickness; the rows of Ca atoms and the rows of Cu atoms alternate along the [010] direction.

It was not possible to image selectively the CuO_2 sublattice separately, in the same area of the specimen, but the Ca sublattice was selectively imaged in Fig. 12b. The difficulty in imaging only the Cu sublattice can be deduced from Fig. 6e: the trace labeled "c" which represents the $(101)^*_{Cu+Ca^T}$ section contains the $20\bar{2}_{Cu}$ spot (small dot) and also the 202_{Ca^T} twin spot (larger dot). The equivalent section with respect to the CuO_2
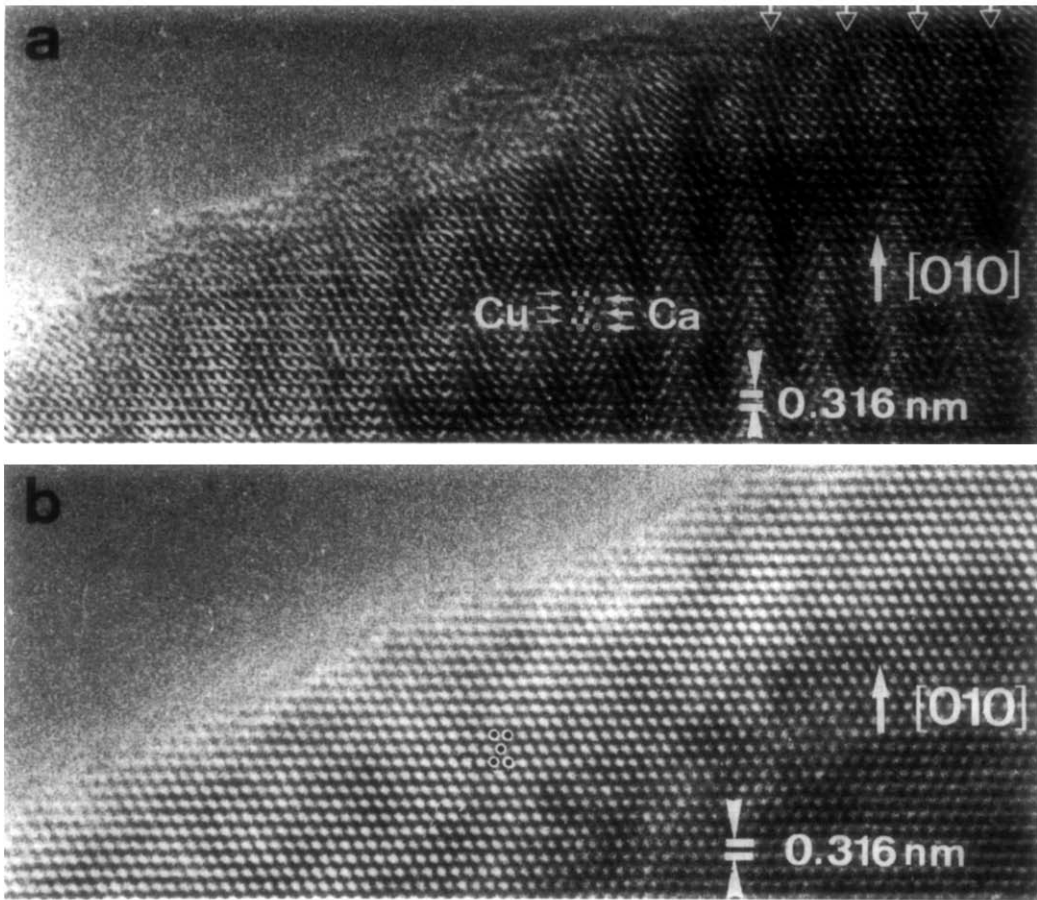
FIG. 12. Selective images of the same area of the $Ca_5Cu_6O_{12}$ crystal which reveal: (a) the mutual modulation of the two substructures when imaging along the common (101)* section. The positions of Cu and Ca atoms in the projected structure are indicated by arrows. The average dot spacing within the Cu rows is $d_{101Cu} = 0.27$ nm, while within the Ca rows it is $d_{101Ca} = 0.29$ nm. (b) The perfect order of Ca atoms in type I stacking when imaging along the $(101)^*_{Ca}$ section. The dot pattern represents the projected structure of the Ca sublattice; it is indicated by black dots. The dot spacing along the horizontal rows is $d_{101Ca} = 0.28$ nm.

orthorhombic lattice would be the $(10\bar{1})^*$ section which contains the 202_{Cu} spot, but also the 202_{Ca}, i.e., the Ca sublattice spot of the twin variant. Therefore, the (101)* and $(10\bar{1})^*$ sections look qualitatively the same. However, by imaging along each of them, the regions with the well-resolved modulated pattern (as in Fig. 12a) of the HREM image usually alternate with regions of poorly resolved modulation, depending on

the volume fraction of the twin variant of the Ca substructure.

On the other hand, selective imaging of the Ca sublattice is easily achieved (Fig. 12b) (by using the Ca reciprocal sublattice section—the trace labeled "d" in Fig. 6), and it reveals the nearly perfect order of the Ca atoms. No regions revealing the type II stacking of Ca atoms are usually found in such selective images, which indicates that

the type I stacking is overwhelmingly present. This is in agreement with the X-ray powder and neutron diffraction data (4) which can be interpreted assuming exclusively that the stacking of Ca is based on the type I monoclinic sublattice within the CuO_2 orthorhombic framework.

7. Computer Simulation

The dynamical diffraction patterns along the $[001]_{Ca}$ zone of the two stackings were simulated using the structure models described under Structural Models, referred to as the monoclinic commensurate superlattice unit cell (1). The copper pattern in the projected structure along the $[001]_{Cu}$ direction, as well as the calculated diffraction pattern, is found to be the same for both Ca stackings; it consists of a primitive rectangle, in complete agreement with the observed electron diffraction pattern (Fig. 5a). The geometry of the diffraction patterns of the Ca sublattice, on the other hand, is different in the two cases. For type I stacking, the diffraction pattern in the $(001)_{Ca}^{*}$ section consists of a primitive rectangular mesh with no 110_{Ca} spot in the center (Fig. 11c). On the other hand, for type II stacking, the diffraction pattern in the $(001)_{Ca}^{*}$ section is built on a rectangular mesh with the same size as that for type I, but it is centered (Fig. 11d). The intensity of the observed $hk0_{Ca}$ spots with h, k = odd reflects the fraction of the type II structure present in the selected area. The calculated diffraction patterns of Fig. 11 are in agreement with the optical diffraction patterns in Fig. 10a. The calculated Ca patterns were obtained by simulating diffraction along the $[105]_m$ zone of the superlattice unit cell (referred to under Structural Considerations) for $Ca_5Cu_6O_{12}$ and by including a shift of one of the two (001) Ca layers over $\frac{1}{2}a_{Ca}$ for the type II structure and no shift for the type I structure.

The diffraction patterns were in turn used to compute (11) images which are shown in

Figs. 11e and 11f for the type I and type II calcium arrangements, respectively. They are selected from an extensive matrix of images for different thicknesses and defocus values. The image parameters in Fig. 11 are Scherzer defocus ($\Delta f = -60$ nm) and thickness ($t = 10.6$ nm). The simulated images in Fig. 11 can be compared with the high-resolution images in the regions A and B in Fig. 10a.

8. Disorder and Diffuse Scattering

The relplanes passing through the spots due to the copper–oxygen sublattice (Fig. 3) are situated in planes parallel with $(100)^{*}$, i.e., perpendicular to the ribbon direction. This suggests that the copper–oxygen ribbons are modulated and that some disorder is present in the phase of the modulation, as was also found for $(Sr-Ca)_{14}Cu_{24}O_{41}$ (12, 13). This is somewhat surprising since we have been given reasons to believe that mainly the calcium sublattice is disordered as a result of twinning and possibly of longitudinal shifts along the "tunnels" of octahedral interstices. The disorder in the copper–oxygen modulation can be understood by assuming that the copper and/or oxygen arrangement is modulated by the calcium chains.

The disorder in the calcium sublattice is due to the presence of the two stacking variants and to twinning of these variants, i.e., to the presence of four structural variants in total. The twin variants produce differently oriented symmetry-related diffraction patterns of which only a fraction of the spots coincide. Also the two stacking variants produce different diffraction patterns, of which half of the spots coincide. The presence of this type of disorder does not produce relplanes. Possibly "relrods" perpendicular to the twin planes, i.e., along c^{*}, might be produced by sequences of thin irregularly spaced twin lamellae.

The relative sharpness of the calcium dif-

fraction spots, even in the presence of the described disorder, is due to the fact that the relative displacements are discrete and equal to one-half or one-third of the Ca–Ca separation, i.e., simply and rationally related to the calcium sublattice. This type of displacement would nevertheless produce relrods along c^* if successive calcium layers parallel to the (001) planes were shifted in a faulted sequence as shown above. Such relrods were indeed observed in tilting experiments.

The nature of diffuse scattering, sometimes observed in the reciprocal space concerning the copper–oxygen sublattice, is different (Fig. 3). The CuO_2 sublattice is modulated by four different calcium arrangements, the period of which is not simply related to the corresponding period of the copper–oxygen sublattice. As a result, depending on which one of the four structural variants is present in a given area, the phase of the modulation of the copper–oxygen framework will be different. This quasi-continuous distribution of the modulation phase of the single copper–oxygen sublattice is responsible for the relplanes observed in the diffraction pattern in Fig. 3.

It is worth noting that the diffuse intensity through the satellite spots indexed 2-2δa, 0, 2 + 2δcl in Ref. (7) (and which we would index as 201_{ct} spots in the cation reciprocal sublattice) suggests the presence of relrods parallel to [001]* or/and relplanes parallel to (100)*, also in the rare-earth cuprates studied in (7), for which the cation/Cu ratio is 4/5. Such relrods reflect heavy twinning visible in Fig. 6, Fig. 7, and Ref. (7).

In the case of relplanes, they should in fact be more pronounced in the diffraction pattern of these compounds since the smaller linear density of the cations in the chains would favor phase disorder in the relative positions of the chains (so-called "pencil disorder"). In the compounds with a smaller cation/Cu ratio of 0.75 such as $Nd_2CaCu_4O_8$, it is evident from the diffuse intensity in Fig. 11 of Ref. (7) that extensive phase disorder (12, 13) is present, leading to an average orthorhombic lattice.

It was shown in Ref. (3) that the relationship between the two sublattices in an intergrowth structure can be imaged by using a section common to both reciprocal lattices. In the present case section (010) is the most suitable. This relationship is represented more clearly, i.e., with higher contrast, by a lattice image than by an atomic resolution image. It is therefore desirable to limit intentionally the resolution by collecting only a limited number of spots belonging in part to each of the two sublattices. Figure 13 was obtained by collecting the set of spots surrounded by the circle in the (010)* section diffraction pattern (inset in Fig. 13). It contains three intense spots due to the copper–oxygen sublattice and three intense close pairs of twin spots connected by streaks, due to the calcium sublattice. The image of Fig. 13 exhibits a horizontal set of straight equidistant fringes, intersected by wavy fringes, roughly along the vertical direction. This vertical set exhibits a number of defects, such as twin-related patches of fringes and dislocation-like configurations. The set of straight equidistant parallel fringes perpendicular to c^* is due to the interference between the spots belonging to the same sublattice. The wavy fringes are due to the interference between beams produced by two different sublattices. The positions of these fringes (i.e., of the intensity extrema) are defined by the phase relationship between the interfering beams. The shift in their positions is thus indicative of a relative shift of the two substructures. The image of Fig. 13 can therefore, in a sense, be interpreted as a map of the relative shifts of the two sublattices. It proves that their relative shifts are along the chain direction, as suggested by the structural models, and vary over the specimen area.

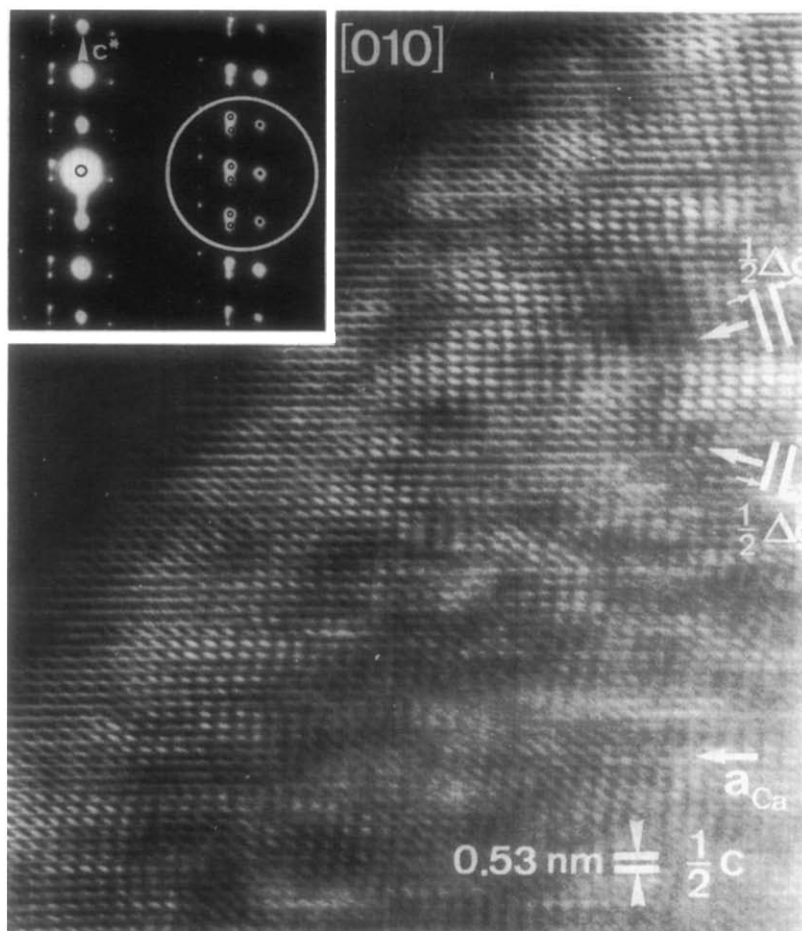Further evidence of local disorder in the phase of the calcium chains with respect to

FIG. 13. Dark-field lattice image of $Ca_5Cu_6O_{12}$ along the [010] zone, using the spots encircled in the diffraction pattern reproduced in the inset (with three Cu and three pairs of twin-related Ca sublattice spots). Note the parallel and straight horizontal fringes and wavy vertical fringes which indicate disorder in phase relations between the two sublattices.

the CuO_2 sublattice is presented in the dark-field lattice image of Fig. 14. The imaged areas exhibit sharply defined coherent modulation twin interfaces (Fig. 14a), as well as ending microtwin lamellae (Fig. 14b). The twinning occurs by a gradual longitudinal shift of the calcium atoms along the a_{Ca} direction.

Changes in the width of the microtwin lamellae imply the presence of "twinning dislocations." In the present case (Fig. 14b), these dislocations are of a peculiar nature

since they affect the calcium sublattice only; the copper–oxygen lattice remains perfect.

Some indications of the nature of the modulation of the CuO_2 sublattice can be derived from the significant anisotropy of the thermal agitation ellipsoid associated with the oxygen atoms according to the neutron diffraction experiments (4). The largest axis of the ellipsoid (1.9 $Å^2$) is found along the direction normal to the plane of the CuO_2 ribbons, whereas the smallest axis (0.4 $Å^2$) is perpendicular to the (001) layer planes;
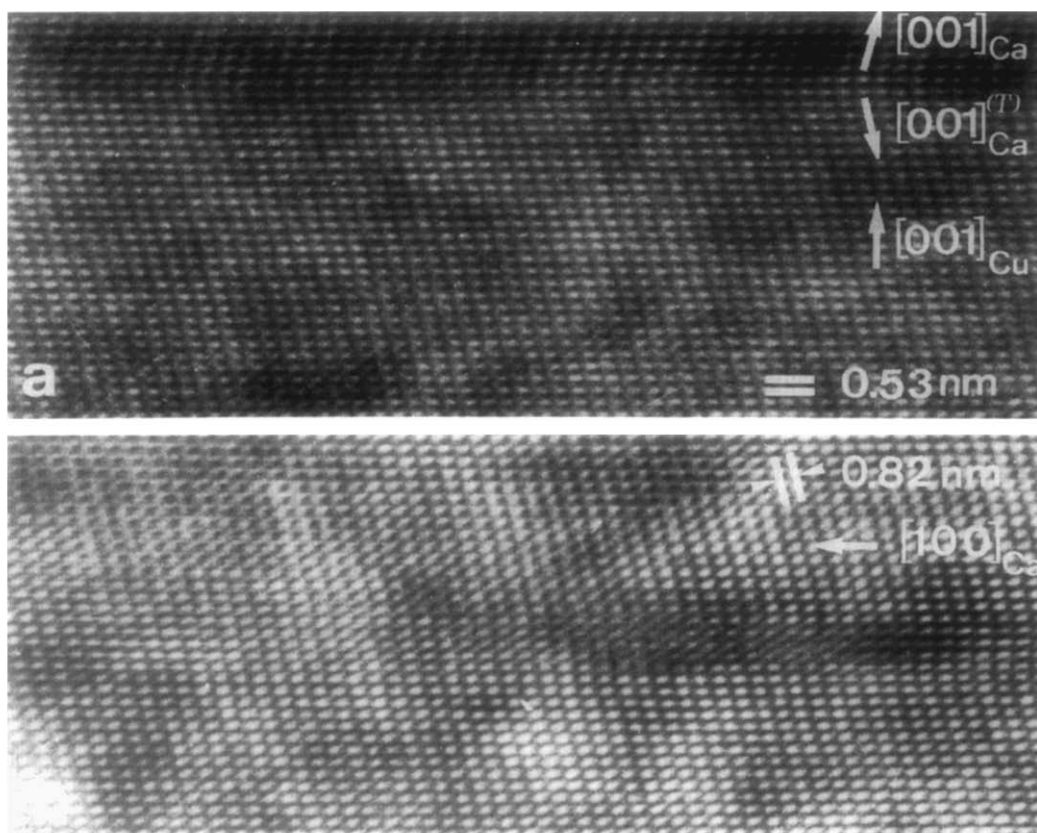
FIG. 14. Dark-field lattice images (under the same conditions as those for Fig. 13) of $Ca_5Cu_6O_{12}$ in the area showing (a) modulation PCP twinning due to the calcium sublattice; (b) the gradual shift of the PCP due to the shift of the calcium chains along an ending microtwin tip.

the intermediate axis (0.8 $Å^2$) is along the chain direction. This type of anisotropy is consistent with a model in which the oxygen atoms are displaced because the Ca^{2+} ions are too small to be accommodated without strain in the center of the oxygen octahedra and probably prefer an off-center coordination. As a result, the adjacent oxygen atoms are presumably displaced toward the calcium ion, the displacements being determined by the exact position occupied by the calcium ion. The latter position varies periodically along the rows of octahedral and/or tetrahedral interstices forming the tunnels (1). The period of these displacements is the smallest common multiple of

the Ca–Ca and Cu–Cu distances along the chain direction. The phase of the displacement waves is essentially determined by the local relative positions of the Ca and CuO_2 sublattices and may thus vary over the specimen, a small relative displacement causing a much larger shift of these phases. As was discussed under Structural Models, the CuO_4 squares in the CuO_2 ribbons are slightly tilted. The tilt angle of the ribbons of CuO_4 planar clusters is presumably modulated with a period equal to that of the calcium chains, causing the apparent thermal agitation of the oxygen atoms as detected by neutron diffraction (4).

9. Composition and Incommensurability

The present results suggest that a commensurate compound $Ca_5Cu_6O_{12}$ exists, and its structure has the monoclinic unit cell with parameters

$$a_m = 1.680; \quad b_m = 0.632 \text{ nm};$$
$$c_m = 1.095 \text{ nm}; \quad \beta_m = 75°.$$

This monoclinic cell is the smallest one containing an integer number of unit cells of both sublattices. The incommensurability of the diffraction patterns can then be considered as being due to deviations from the above composition: $Ca_{5+x}Cu_6O_{12}$. The incommensurability was related to "phase slips" in the structure as observed by high-resolution electron microscopy (1). A phase slip corresponds in fact to the correlated insertion of additional calcium ions in the tunnels of the CuO_2 framework. This operation will decrease the average separation of the Ca ions, which tend to be spaced uniformly as a result of Coulomb repulsion. For computational purposes we can, however, assume that a sequence of five Ca atoms which occupies a length of tunnel equal to six Cu–Cu separations consists of five Ca ions with a spacing equal to that of Cu atoms, followed by a vacancy. Suppose now that after every n such 5Ca/6Cu sequences, a sequence consisting of six Ca ions and no vacancy is inserted; then the bulk composition ratio Ca/Cu would become $(5n + 6)/(n + 1)6$. With this assumption the nonstoichiometry index x in $Ca_{5+x}Cu_6O_{12}$ can be expressed as a function of n, $x(n) = 1/(n + 1)$, with the above-mentioned meaning of n. Furthermore, the ratio of the average Ca–Ca spacing over Cu–Cu spacing as a function of composition would be $6(n + 1)/(5n + 6) = 6/(5 + x)$.

In the limiting case $n \rightarrow 0$, corresponding to no insertion of 6Ca/6Cu sequences, the composition would be the above-mentioned $Ca_5Cu_6O_{12}$ ($x = 0$). In the other limiting case, for $n \rightarrow 0$, corresponding to the pres-

ence of only 6Ca/6Cu sequences, the composition would be $CaCuO_2$ with $x = 1$, and the Ca–Ca spacing would be equal to the Cu–Cu spacing. This is apparently unstable, the repulsion between the Ca ions being excessive; from the average Ca–Ca spacing in the chemically related compounds $(Ca_{0.85}Sr_{0.15})CuO_2$ (8), Ca_2CuO_3 (14), and $CaCu_2O_3$ (15), it seems that it is impossible to pack calcium atoms closer than roughly 0.32 nm (6). Therefore the considered structure is, as expected, unstable for the n values 0, 1, and 2 (x equals 1, 0.5, and 0.33) and the corresponding Ca/Cu ratios $6/6 = 1$, $5.5/6 = 0.91$, and $5.3/6 = 0.88$, since these values imply that the Ca–Ca spacings would be 0.280, 0.306, and 0.315 nm, respectively. The incommensurability discussed in (1) and (2) can thus also be considered as being due to nonstoichiometry in $Ca_{5+x}Cu_6O_{12}$ for $x = 0.125$ ($n = 7$) and $x = 0.143$ ($n = 6$), which closely correspond with the nominal composition $Ca_{0.85}CuO_2$. The value of 0.85 seems to be the upper limit of the Ca/Cu ratio (4) for the $Ca_{5+x}Cu_6O_{12}$ structure.

Although we have not found a structure which would correspond to a phase having a smaller Ca/Cu ratio, superstructures with compositions $Ca_4Cu_5O_{10}$ and $(Ca–RE)_4 Cu_5O_{10}$ (5–7) were reported to have a superlattice analogous to the one for $Ca_{0.85} CuO_2$ (1), and, therefore, we can speculate that our considerations, based on the two sublattice intergrowth structure, are applicable to all these compounds.

However, it is possible to envisage a number of compositions leading to analogous commensurate structures (corresponding to $Ca_{5+x}Cu_6O_{12}$), with different coincidence sequences ($Ca_{4+x}Cu_5O_{10}$, $Ca_{3+x}Cu_4O_8$, . . .). For a cation/Cu composition ratio equal to 0.583 in $(Sr–Ca)_{14}Cu_{24}O_{14}$, a different structure was found(16, 17) but also, in that case, the structure can be described as an intergrowth built on two different sublattices (12, 18).

10. Conclusions

Since the publication of our previous papers on the composition-driven modulated structure of $Ca_{0.85}CuO_2$ (1, 2), the method of selective imaging of the substructures in intergrowth structures has been developed (3). As pointed out in (1), the structure of $Ca_{0.85}CuO_2$ can be described with respect to two geometrically distinct sublattices: a calcium sublattice and a copper–oxygen sublattice. The method of selective imaging can thus be applied to the present case. This method of analyzing the structure has made it possible to obtain some additional information.

It was confirmed that commensurate as well as incommensurate diffraction patterns occur. In this paper we have focused attention mainly on the material producing a commensurate diffraction pattern and which was therefore assumed to have a commensurate structure with ideal composition $Ca_5Cu_6O_{12}$. The ratio of the Ca–Ca separation a_{Ca} to the Cu–Cu separation a_{Cu} is then exactly $a_{Ca}/a_{Cu} = 6/5$.

It is suggested that analogous reasoning could be applied to the wider range of compositions down to $Ca_4Cu_5O_{10}$ or to $Ca_3Cu_4O_8$ (and even for intermediate noninteger stoichiometry $(Ca–RE)_xCuO_2$), for which the a_{Ca}/a_{Cu} ratio would correspond to 5/4 or to 4/3 (or $a_{cation}(x)/a_{Cu} = 1/x$), respectively.

We have given evidence for the occurrence of two different stacking modes of the calcium chains within the face-centered orthorhombic copper–oxygen framework. The calcium chains always have a staggered arrangement within the (001) layers, but the stacking along the [001] direction of such (001) layers can take place according to two different modes related by a vector $\frac{1}{2}[100]a_{Ca}$. In the first mode (type I, . . .ABAB. . .) the chains are staggered also along the [001] direction, forming a non-primitive all-face-centered monoclinic lattice. In the second mode (type II, . . .AA. . . or . . .BB. . .) they are verti-cally stacked, forming a C-base-centered monoclinic Bravais lattice. "Islands" exhibiting type II stacking are found by high-resolution electron microscopy to be embedded in a "sea" of the type I stacked matrix.

In view of the evidence found with electron diffraction, an attempt was made to provide evidence for the type II stacking mode in the X-ray diffraction patterns. It turns out that all observed peaks can be satisfactorily accounted for on the basis of the type I structure. This is not surprising since the electron microscopic observations have shown that the type II structure occurs only in small islands embedded in type I material.

The presence of $hk0$ spots with h = even and k = odd, in the selective diffraction pattern associated with the copper–oxygen substructure, was interpreted as being caused by a small tilt of the ribbons of CuO_4 clusters with respect to the (010) plane. This interpretation is consistent with the elongated shape along [010] of the thermal agitation ellipsoids, associated with the oxygen atoms, as determined by neutron diffraction. It is moreover suggested that the magnitude of the tilt angle is modulated by the calcium chains. The phase of this modulation will thus depend on the phase of the calcium chains, which was shown to vary over the specimen area as a consequence of the presence of two stacking modes and of their associated twin modes, leading to four stacking variants. As a result, the copper–oxygen sublattice is modulated, exhibiting a spectrum of phases and thereby leading to the presence of diffuse relplanes perpendicular to the chain direction in the diffraction patterns.

Acknowledgments

ductors initiated by the Belgian State Science Policy Office under Contract SU/03/017.

References

1. O. MILAT, G. VAN TENDELOO, S. AMELINCKX, T. G. N. BABU, AND C. GREAVES, *J. Solid State Chem.* **97,** 405 (1992).

2. O. MILAT, G. VAN TENDELOO, S. AMELINCKX, T. G. N. BABU, AND C. GREAVES, *Solid State Commun.* **79,** 1059 (1991).

3. O. MILAT, G. VAN TENDELOO, AND S. AMEL- INCKX, *Ultramicroscopy,* in press.

4. T. G. N. BABU AND C. GREAVES, *Mater. Res. Bull.* **26,** 449 (1991).

5. R. S. ROTH, C. J. RAWN, J. J. RITTER, AND B. P. BURTON, *J. Am. Ceram. Soc.* **72,** 1545 (1989).

6. T. SIEGRIST, R. S. ROTH, C. J. RAWN, AND J. J. RITTER, *Chem. Mater.* **2,** 192 (1990).

7. P. K. DAVIES, *J. Solid State Chem.* **95,** 365 (1991).

8. T. SIEGRIST, S. M. ZAHURAK, D. W. MURPHY, AND R. S. ROTH, *Nature* **334,** 231 (1988).

9. M. G. SMITH, A. MANTHIRAM, J. ZOU, J. B. GOOENOUGH, AND J. T. MAKERT, *Nature* **351,** 549 (1991).

10. S. KUYPERS, G. VAN TENDELOO, J. VAN LAN- DUYT, AND S. AMELINCKX, *Acta Crystallogr. A* **45,** 291 (1989).

11. D. VAN DYCK AND W. COENE, *Ultramicroscopy* **15,** 29 (1984).

12. O. MILAT, G. VAN TENDELOO, S. AMELINCKX, R. MEHBOD, AND R. DELTOUR, submitted for pub- lication.

13. X. J. WU AND S. HORIUCHI, *Acta Crystallogr. A* **47,** 11 (1991).

14. C. TESKE AND HK. MÜLLER-BUSHBAUM, *Z. An- org. Allg. Chem.* **379,** 234 (1970).

15. C. TESKE AND HK. MÜLLER-BUSHBAUM, *Z. Anorg. Allg. Chem.* **370,** 134 (1969).

16. E. M. MCCARRON, III, M. A. SUBRAMANIAN, J. C. CALABRESE, AND R. L. HARLOW, *Mater. Res. Bull.* **23,** 1355 (1988).

17. K. KATO, E. TAKAYAMA-MUROMACHI, K. KOSUDA, AND Y. UCHIDA, *Acta Crystallogr. C* **44,** 1881 (1988).

18. X. J. WU, E. TAKAYAMA-MUROUCHI, S. SUEHARA, AND S. HORIUCHI, *Acta Crystallogr. A* **47,** 727 (1991).